Universiteit
Leiden
The Netherlands

On preoperative systemic treatment of muscle-invasive bladder cancer

Dorp, J. van

Citation
Dorp, J. van. (2025, January 10). *On preoperative systemic treatment of muscle-invasive bladder cancer*. Retrieved from https://hdl.handle.net/1887/4175499

Version:	Publisher's Version
License:	Licence agreement concerning inclusion of doctoral thesis in the Institutional Repository of the University of Leiden
Downloaded from:	https://hdl.handle.net/1887/4175499

Note: To cite this publication please use the final published version (if applicable).

CHAPTER 4

Platinum-based chemotherapy induces opposing effects on immunotherapy response-related spatial and stromal biomarkers in the bladder cancer microenvironment

Jeroen van Dorp, Maksim Chelushkin, Sandra van Wilpe, Iris M. Seignette, Jan-Jaap J. Mellema, Maartje Alkemade, Alberto Gil-Jimenez, Dennis Peters, Wim Brugman, Chantal F. Stockem, Erik Hooijberg, Annegien Broeks, Bas W.G. van Rhijn, Laura S. Mertens, Antoine G. van der Heijden, Niven Mehra, Maurits L. van Montfoort, Lodewyk F. A. Wessels, Daniel J. Vis, and Michiel S. van der Heijden

Submitted to Clinical Cancer Research

ABSTRACT

PURPOSE

Platinum-based chemotherapy and immune checkpoint inhibitors are key components of systemic treatment for muscle-invasive and advanced urothelial cancer. The ideal integration of these two treatment modalities remains unclear as clinical trials have led to inconsistent results. Modulation of the tumor-immune microenvironment by chemotherapy is poorly characterized. We aimed to investigate this modulation, focusing on potential clinical implications for immune checkpoint inhibitor response.

EXPERIMENTAL DESIGN

We assessed immune cell densities, spatial relations, and tumor/stromal components from 116 urothelial bladder cancer patients (paired data for 95 patients), before and after platinum-based chemotherapy.

RESULTS

Several published biomarkers for immunotherapy response changed upon chemotherapy-treatment. The intratumoral $CD8^+$ T-cell percentage increased after treatment and was associated with increased TNFα-via-NFκB signaling. The percentage of PD-$L1^+$ immune cells was higher after chemotherapy. An increase in chemo-induced changes that potentially inhibit an anti-tumor immune response was also observed, including increased fibroblast-based TGF-β signaling and distances from immune cells to the nearest cancer cell. The latter two parameters correlated significantly in post-treatment samples, suggesting that TGF-β signaling in fibroblasts may play a role in spatially separating immune cells from cancer cells. We examined specific chemotherapy regimens and found that treatment with methotrexate, vinblastine and adriamycin was associated with an increase in the macrophage cell percentage. Gemcitabine-containing chemotherapy were associated with upregulation of fibroblast TGF-β signaling.

CONCLUSIONS

The opposing effects of platinum-based chemotherapy on the immune cell composition and stromal context of the tumor-immune microenvironment may explain the inconsistent results of clinical trials investigating chemotherapy and immune checkpoint inhibitor combinations in bladder cancer.

TRANSLATIONAL RELEVANCE

In various tumor types, successful synergy of chemotherapy and immune checkpoint inhibitors (ICI) has been established, but in muscle-invasive bladder cancer (MIBC), clinical trials yielded inconsistent results. Therefore, understanding chemotherapy-induced changes in the tumor-immune microenvironment (TIME) of MIBC is highly relevant. To investigate them, we collected and analyzed a large dataset of paired pre- and post-platinum-treatment tumor samples. We demonstrate that platinum-based neoadjuvant chemotherapy (NAC) is associated with promoting TIME characteristics previously shown to relate to both ICI response and resistance. The latter includes fibroblast-based TGF-β signaling and median distances from $CD8^+$ T-cells and macrophages to their nearest cancer cells. This suggests that responses to ICI in MIBC after platinum-based NAC might be improved by adding TGF-β inhibitors or bispecific antibodies promoting spatial rearrangements of immune and cancer cells. Finally, our data suggests differences between MVAC and gemcitabine-containing platinum-based regimens in their effects on the bladder TIME.

INTRODUCTION

Cisplatin-based neoadjuvant chemotherapy (NAC) followed by radical cystectomy is recommended for patients with muscle-invasive bladder cancer (MIBC)[1]. Accelerated methotrexate, vinblastine, adriamycin and cisplatin (MVAC) and cisplatin-gemcitabine are the two most commonly used NAC regimens for MIBC[2]. Despite a pathological complete pathological response rate (pCR) of 25-42%, cisplatin-based NAC is associated with only a 5-8% absolute increase in 5-year overall survival (OS) when compared to radical cystectomy alone[3,4,5]. Recently, the CheckMate-274 trial showed that adjuvant treatment with nivolumab (PD-1 inhibitor) significantly increased disease-free survival (DFS) for patients with residual MIBC or lymph node involvement[6]. Exploratory analyses revealed a notable improvement of DFS for patients who were previously treated with cisplatin-based NAC (hazard ratio (HR): 0.52; 95% CI: 0.38-0.71 for nivolumab vs. placebo), while those who did not receive NAC appeared to have limited benefit (HR: 0.92; 95% CI: 0.69-1.21).

In the metastatic setting, improved clinical outcomes have been observed in patients treated with avelumab (PD-L1 inhibitor) maintenance therapy after platinum-based chemotherapy, similarly suggesting a benefit of sequential treatment with chemo- and immunotherapy[7]. Clinical trials exploring concurrent chemotherapy and immune checkpoint inhibitors (ICI) have shown mixed results. In the IMvigor130 trial, atezolizumab, combined with platinum-based chemotherapy as first-line treatment for advanced urothelial cancer, improved progression-free survival (PFS) compared to chemotherapy alone, although the improvement in OS (final 1-sided p-value=0.023) did not reach statistical significance (final OS efficacy boundary: P=0.021)[8,9]. In an exploratory analysis, a more pronounced effect of atezolizumab on OS (and PFS) was observed in the cisplatin-treated

subgroup (HR for OS: 0.73; 95% CI: 0.54-0.98) versus the carboplatin-treated subgroup (HR for OS: 0.91; 95% CI: 0.75-1.10)[10]. The CheckMate-901 study specifically tested the addition of nivolumab to cisplatin-based chemotherapy, reporting positive results for the primary endpoints OS (HR=0.78) and PFS (HR=0.72)[11]. These findings suggest that the combination of ICI with cisplatin-based chemotherapy may be more effective than with carboplatin-based chemotherapy. Conversely, the addition of pembrolizumab to first-line platinum-based chemotherapy in the KEYNOTE 361 study did not significantly improve PFS or OS by central review in the unselected population per the prespecified p-value boundaries[12]. However, hazard-ratios for PFS were 0.78 (95% CI: 0.65–0.93) in the total population and 0.67 (95% CI: 0.51–0.89) in the choice-of-cisplatin subgroup[12]. Although clinical trials suggest potential synergy between platinum-based chemotherapy and ICI (either sequential or concurrent), results have not been unequivocally positive. Additionally, the positive results may partly be explained by earlier ICI initiation, as only a subset of patients (25-48%) in the standard arms of the chemo-immunotherapy trials in the advanced urothelial cancer setting received ICI as subsequent therapy[7,8,11,12]. Given the disappointing results in several trials testing concurrent platinum-based chemotherapy and ICI, particularly when combining carboplatin-based chemotherapy with ICI, a negative interaction between chemotherapy and ICI (e.g. by immune suppression) in a subset of patients cannot be excluded[8,12].

Here, we investigate the changes in the bladder cancer tumor microenvironment (TIME) induced by platinum-based NAC, focusing on potential implications for immunotherapy treatment. For this purpose, we collected and analyzed RNA-seq, multiplex immunofluorescence (mIF), and immunohistochemistry (IHC) data of tumor tissue from MIBC patients before and after treatment with platinum-based chemotherapy.

RESULTS

COHORT AND DATA DESCRIPTION

We retrospectively included 183 MIBC patients treated with platinum-based NAC followed by radical cystectomy (Supplementary Fig. 1, Methods). Patients achieving a pCR to NAC have a favorable clinical outcome and are therefore less likely to benefit from additional ICI treatment; these patients were not included in the various adjuvant ICI studies for this reason[6]. Furthermore, as all tumor cells will have been eliminated in patients with a pCR after neoadjuvant chemotherapy and prior to tissue collection, a reliable TIME analysis cannot be conducted in these patients. Therefore, regardless of nodal status, only patients with remaining viable tumor tissue at cystectomy (≥ypT1) were included (Supplementary Fig. 1). Tissue samples from 130 patients were subjected to analysis. We collected pre-treatment transurethral resection of the bladder tumor (TUR-BT) tissue at diagnosis (baseline) and post-treatment cystectomy tissue (resected tumor bulk) from each patient (Fig. 1A). In total 116 unique patients represented by at least one sample of one data type (mIF, IHC, RNA-seq) were included in our dataset. Sixty-two (53%) patients

had clinically node-negative disease at baseline (cT2-4aN0), and fifty-four (47%) patients were clinically node-positive (cT2-4aN1-3, Fig. 1B). Cisplatin was the most frequently used platinum-based treatment agent (78% of patients). Other patients were treated with carboplatin (12%) or switched their platinum agent during neoadjuvant treatment due to toxicity (8%). Of note, whereas cisplatin-based chemotherapy is the standard treatment in the neoadjuvant setting, some locoregionally advanced cis-ineligible patients were treated with carboplatin-based induction therapy and had consolidative surgery in case of a clinical response. As the active metabolites between these platinum-agents are similar[13] and questions regarding a potential difference in immune-induction remain to be answered, we included both platinum agents. Besides platinum, the treatment regimen included gemcitabine (in 66% of patients) or methotrexate, vinblastine, and doxorubicin (MVAC, 28%), or both at different time points (3%). The majority of patients (78%) received four cycles of NAC, while a subset received fewer (10%) or more (10%) than four cycles (Fig. 1B). The processed sample counts for each experimental technique and timepoint are shown in Fig. 1 C and D. Due to failed quality control, not all patients had both TUR-BT and cystectomy samples processed successfully. The final numbers of paired samples included 85 pairs of multiplex immunofluorescence (mIF), 76 pairs of RNA-sequencing, and 79 pairs of PD-L1 immunohistochemistry (IHC). In 59 patients, all three analyses could be performed on paired samples (Fig. 1E).

CHEMOTHERAPY-INDUCED CHANGES IN ICI RESPONSE BIOMARKERS

Abundance of tumor-infiltrating $CD8^+$ T-cells, PD-L1 expression, and gene signatures related to T-cell immunity (e.g., IFNγ and effector $CD8^+$ T-cell gene signatures) are biomarkers commonly associated with ICI response in cancer, including MIBC[14,15,16]. In our cohort, the $CD8^+$ T-cell percentage (mIF) increased in the tumor area (P=0.015) and adjacent stroma (P=0.017; Methods) as well as in their combined area (P=0.00076; Fig. 2A-C) upon chemotherapy treatment. The percentage of PD-L1 positive immune cells (IC), determined by IHC, increased after treatment (P=0.00033; Fig. 2D), while the percentage of PD-L1 positive tumor cells (TC) and the PD-L1 combined positivity score (CPS) remained unchanged (Fig. 2E, F). A fibroblast-based TGF-β signaling gene signature was previously associated with ICI resistance in MIBC in subsets of patients[14,15,17]. The single-sample gene set enrichment analysis (ssGSEA) score of this signature increased upon chemotherapy treatment in our cohort (P=1.2 * 10^{-8}; Fig. 2G). No difference in IFNγ and effector $CD8^+$ T-cell gene signatures between pre- and post-chemotherapy tumor tissue were detected (Fig. 2 H, I). These results demonstrate that features both positively ($CD8^+$ T-cell percentage, PD-L1 IC score) and negatively (TGF-β signaling in fibroblasts) associated with ICI response in MIBC increased upon platinum-based chemotherapy.

A

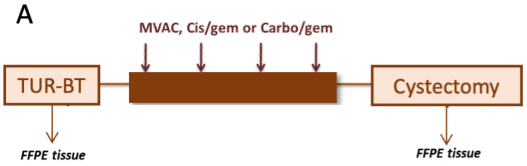

B

Patient and tumor characteristics	Total (n = 116)
Median age, years (range)	62 (31-86)
Male sex, n (%)	83 (72%)
Clinical classification at baseline • cT2-4N0 • cT2-4N1-3	 62 (53%) 54 (47%)
Pathological classification at cystectomy • ypT2-4N0-x • ypT1-4N1-3	 62 (53%) 54 (47%)
Platinum chemotherapy agent • Cisplatin • Carboplatin • Switched • Unknown	 91 (78 %) 14 (12%) 9 (8%) 2 (2%)
Chemotherapy regimen • MVAC • Gemcitabine + cisplatin or carboplatin • Switched • Unknown	 33 (28%) 77 (66%) 4 (3%) 2 (2%)
Total number of chemotherapy cycles • 4 • <4 • >4 • Unknown	 90 (78%) 12 (10%) 12 (10%) 2 (2%)

C

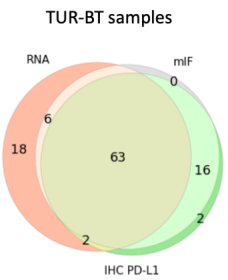

D

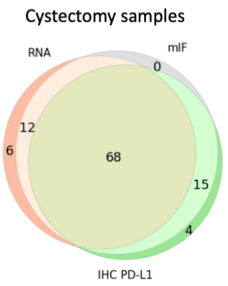

E

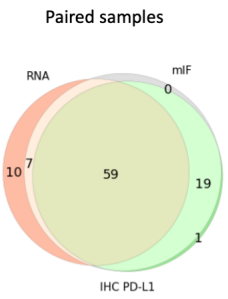

Figure 1 | Patient cohort characteristics and collected data. A, Treatment scheme. **B**, Patient and tumor characteristics. **C**, Availability of pre-treatment (TUR-BT) data by type. **D**, Availability of post-treatment (cystectomy) data by type. **E**, Number of sample pairs (TUR-BT-cystectomy from the same patient) available.

COMPREHENSIVE ASSESSMENT OF TIME CHANGES UPON CHEMOTHERAPY TREATMENT

Next, we aimed to better understand the effect of platinum-based chemotherapy on the bladder cancer TIME in a more comprehensive and unsupervised manner. We assessed alterations in the cellular immune cell composition by mIF and transcriptional changes through RNA-sequencing data by comparing pre- vs post-chemotherapy samples. Because we used different sample types for our analyses, which are transurethral resection (TUR-BT) samples as pre-chemotherapy tissue and radical cystectomy samples after chemotherapy, we aimed to identify and mitigate possible biases in the mIF data analysis. After finding a difference in the total cell density between the sample types (Supplementary Fig. 2A), we proceeded with cell percentages instead of raw densities to minimize a possible confounding effect of the sample type. Comparison of TIME cell percentages assessed by mIF analysis (normalized densities) showed that, besides the $CD8^+$ T-cell percentage increase after chemotherapy, the macrophage cell percentage increased as well (adj. P=0.016; Fig. 3A). Boxplots showing cell percentages and raw densities of all cell types identified by our mIF panel between TUR-BT and cystectomy sample sets are shown in Supplementary Fig. 3. Gene set enrichment analysis (GSEA) performed with the Hallmark gene sets[18] on the differentially expressed genes before and after treatment showed (among others) a strong upregulation of epithelial-mesenchymal transition (EMT; adj. P=5.5 * 10^{-27}) and TNFα-via-NFκB signaling (adj. P=3.0 * 10^{-33}; Fig. 3B). Of note, EMT signaling was previously associated with ICI resistance in urothelial cancer[19]. We recently showed that a shorter distance from macrophages and $CD8^+$ T-cells to their first-nearest neighboring (1-NN) cancer cells at baseline was positively associated with pre-operative combination ICI response in an analysis of the NABUCCO (MIBC) and IMCISION (head and neck cancer) trials[17,20,21]. Following the same approach, we quantified the median 1-NN distances for each spatial relationship as identified by our mIF panel (refer to the Methods section for more details). To identify a possible bias between the sample types, we analyzed the cell-type-agnostic 1-NN median distances and established that they were similar between TUR-BTs and cystectomies (Methods, Supplementary Fig. 2B), suggesting no bias in the analysis of 1-NN median distances.

A comparison of paired cystectomies and TUR-BTs showed that all five immune cell types tested (CD8 T-cells, macrophages, Tregs, helper T-cells, and B-cells) were, on average, further away from their 1-NN cancer cells after chemotherapy treatment compared to the pre-treatment sample (Fig. 3C), including $CD8^+$ T-cells (adj. P=1.6 * 10^{-5}) and macrophages (adj. P=1.5 * 10^{-5}; Fig. 3D). Thus, whereas the percentages of cells with potential anti-tumor immune activity increased upon chemotherapy, immune cells were (on average) further from the nearest neighboring cancer cells. This increased distance suggests that their anti-tumor activity may be impeded. Fold changes in $CD8^+$ T-cell percentages did not correlate to the fold changes in median distances from $CD8^+$ T-cells to 1-NN cancer cells (Supplementary Fig. 4). Therefore, in many sample pairs, only one of the two characteristics increased (Supplementary Fig. 4, examples in Fig. 3E, F). Still, in some sample pairs, both characteristics became higher (Supplementary Fig. 4, examples in Fig. 3G).

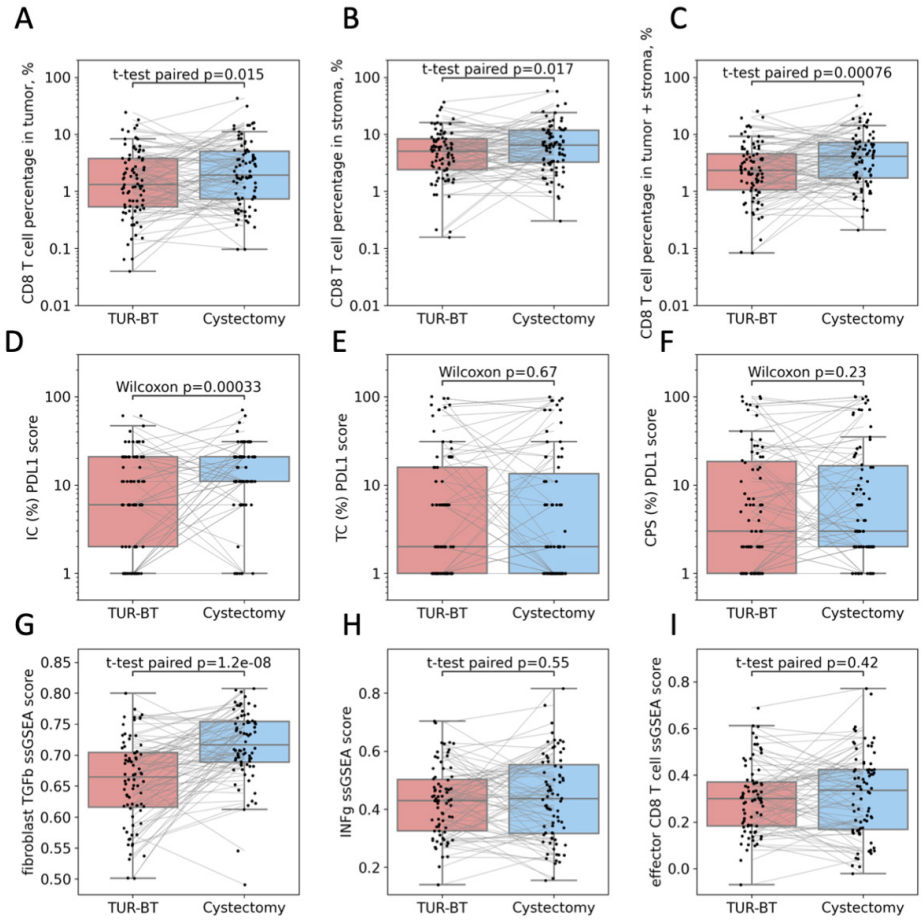

Figure 2 | Changes associated with platinum-based chemotherapy. A-C, $CD8^+$ T-cell percentage determined by mIF in the tumor (A), stromal areas (B) and full analyzed area (C). **D**, Percentage of PD-L1 positive immune cells (IC) determined by IHC. **E**, Percentage of PD-L1 positive tumor cells (TC) determined by IHC. **F**, PD-L1 combined positivity score (CPS) determined by IHC. **G**, ssGSEA score of the fibroblast-based TGF-β signaling gene signature from[14]. **H, I**, ssGSEA score of Interferon gamma and $CD8^+$ T-cells effector gene signatures. ssGSEA, single-sample gene set enrichment analysis. *IQR: interquartile range*.

CORRELATION ANALYSES SUGGEST DIFFERENT TIME RESPONSE PATTERNS TO CHEMOTHERAPY

Next, we investigated whether changes in stromal (fibroblast TGF-β and EMT) and inflammation-related (TNFα-via-NFκB) signatures correlated with specific changes in the TIME immune cell composition upon treatment with chemotherapy. For this analysis, we considered immune cell percentages and distances that changed after chemotherapy treatment, i.e., $CD8^+$ T-cell and macrophage percentages and all five immune-to-cancer cell distances (Fig. 3 A, C), as well as the PD-L1-positive immune cell percentage (Fig. 1D). For the correlation analysis, we used the Kendall

τ-*b* correlation coefficient (because of ties in the PD-L1 data). Results of Pearson correlation analysis excluding PD-L1 IC data are shown in Supplementary Fig. 5 A-C. We found an association between the increase in $CD8^+$ T-cell percentage and upregulation of TNFα-via-NFκB signaling upon chemotherapy (τ-*b* = 0.29, *P*=0.00048; Fig. 4A, Supplementary Fig. 6A). The TNFα-via-NFκB signature and $CD8^+$ T-cell percentage also correlated significantly after chemotherapy, i.e., within the cystectomy sample set (τ-*b* = 0.23, *P*=0.0021; Fig. 4B, Supplementary Fig. 6B) and before chemotherapy, i.e., within the TUR-BT sample set (τ-*b* = 0.24, *P*=0.0042; Fig. 4C, Supplementary Fig. 6C). These results suggest that a subset of patients experienced an induction of T-cell immunity upon platinum-based chemotherapy, e.g., patients with a higher than median change in TNFα-via-NFκB signaling showed a higher fold change in $CD8^+$ T-cell infiltration (*P*=0.014; Fig. 4D). On the other hand, the fibroblast-based TGF-β signaling positively correlated with higher distances (but not densities) from each immune cell type to their nearest cancer cell within post-treatment samples (Fig. 4B, F). Also, a negative correlation was observed between these distances and the PD-L1 IC score (Fig. 4B). Furthermore, we investigated the correlation between PD-L1 IC and fibroblast TGF-β signaling, and found a significantly negative correlation (Supplementary Fig. 6D, □-*b* = -0.27, *P*=0.0022). When comparing high vs. low PD-L1 IC in post-treatment samples as assessed by the median PD-L1 IC score (11%), the IC-low subset showed a higher fibroblast-derived TGF-β signaling score (Fig. 4E, right) and larger distances from immune cells to their nearest cancer cells (regardless of their density; Fig. 4G, right). This was not observed when comparing TUR-BT samples split by the baseline PD-L1 IC median (6%; Fig. 4 E, G, left).

In our previous work with NABUCCO samples, we found a negative correlation between pathologic response to pre-operative immunotherapy and both fibroblast TGF-β signaling[17] and 1-NN $CD8^+$ T-cell-cancer cell distances[21]. Therefore, we expect the TIME in patients belonging to the subset having post-chemotherapy high TGF-β signaling and 1-NN CD8-cancer cell distance and low PD-L1 IC score to be less likely to support response to ICI. The associations found between TGF-β, PD-L1 IC positivity, and immune-to-cancer cell distances in the post-treatment set appeared to be weaker or absent before treatment (Fig. 4C). We formally tested which correlations changed upon treatment using Fisher's z-transformation of the equivalent Pearson correlations (Methods) and found a statistically significant change (FDR < 10%) for the immune cell distances to 1-NN cancer cells and PD-L1 IC positivity (Supplementary Fig. 7, an example for CD8 T-cells and IC is shown on Supplementary Fig. 6E, F). Although the correlation coefficient between the macrophage-to-cancer-cell distance and PD-L1 IC score increased significantly (with FDR level < 5%), it was the pair with the weakest resulting correlation in the cystectomy set (Fig. 4B). These results suggest that the percentage of PD-L1 positive cells among immune cells is higher when they are closer to their nearest neighboring cancer cells, and this relation appears only after chemo-treatment. For $CD8^+$ T-cell-to-cancer-cell distances, this is illustrated in Fig. 4G with the PD-L1 IC score binarized by medians. distance between groups of TUR-BT and cystectomy samples with the PD-L1 IC score lower and higher than the TUR-BT median and the cystectomy median correspondingly.

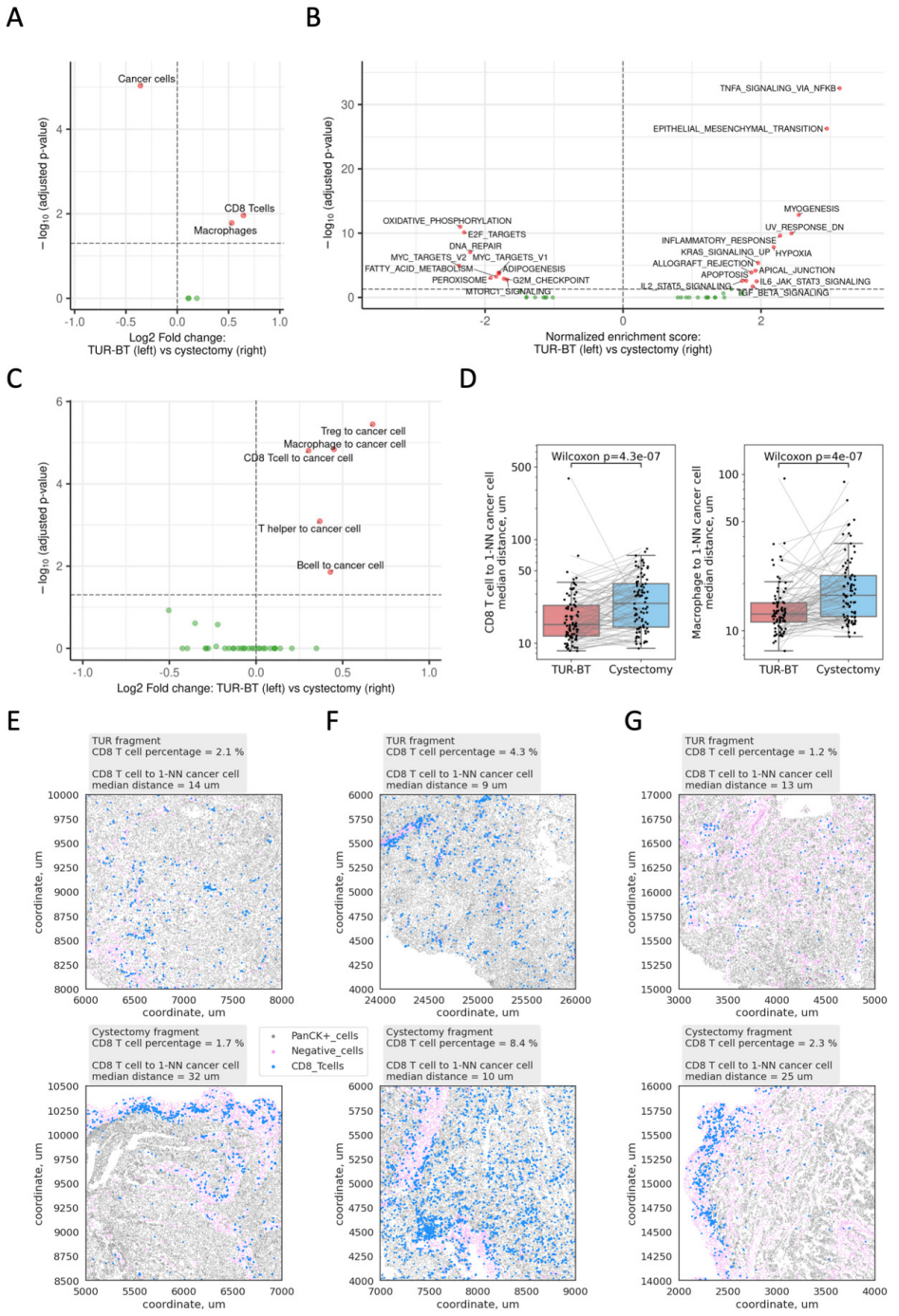

Figure 3 | A, mIF-based cell percentages compared between post- and pre-treatment. **B**, GSEA results for hallmark gene signatures. **C**, 1-NN median distances calculated from fitting Weibull distribution to the mIF data and compared between post- and pre-treatment. **D**, Comparison of median distances from $CD8^+$

T-cells to 1-NN cancer cells and from macrophages to 1-NN cancer cells between post- and pre-treatment. **E-G**, Examples of slide fragments for corresponding TUR-BT and cystectomy samples recreated based on cell coordinates and labels. Only CD8⁺ T-cells (blue), cancer cells (grey), and DAPI-positive cells negative with the other markers (purple) are shown. P-values shown in A and C are Wilcoxon test p-values adjusted with Bonferroni correction for multiple testing.

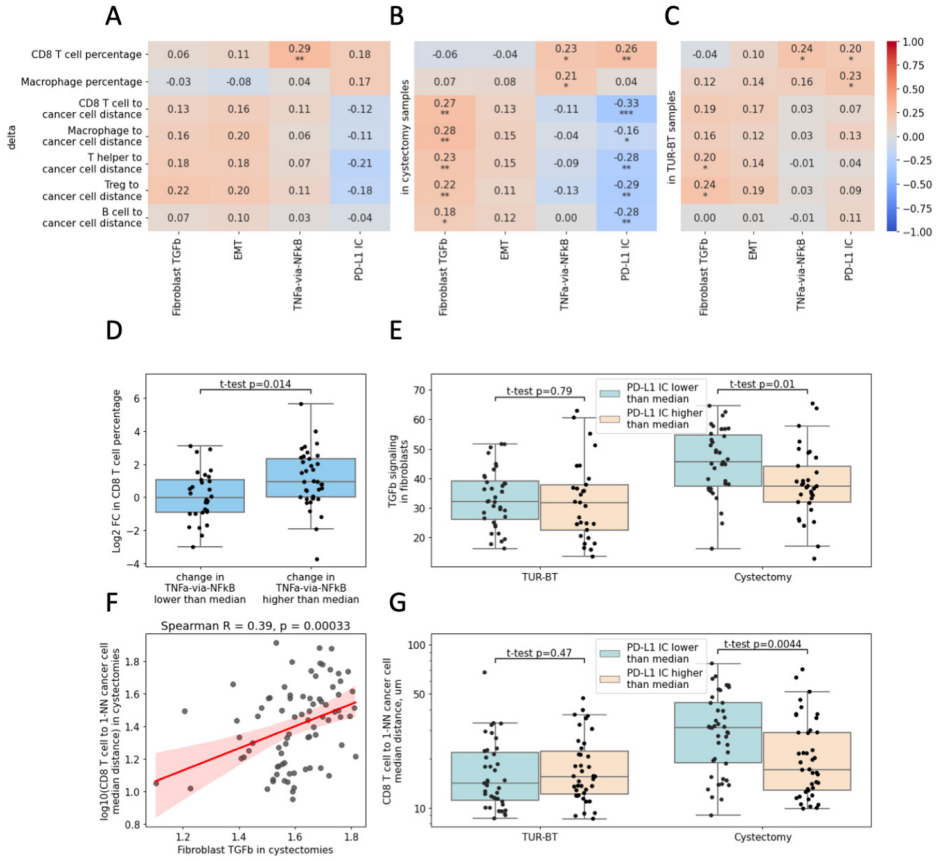

Figure 4 | A-C, Correlation analysis of parameters altered by the chemo-treatment between different data modalities. RNA-Seq and IHC are shown on the x-axis and mIF is shown on the y-axis. Kendall τ-b correlation coefficients are shown and indicated by colors. Stars denote p-values for the correlation coefficients to be non-zero assessed by the distribution of τ (two-sided test): *: p<0.05, **: p<0.01, ***: p<0.001. P-values are FDR-adjusted for multiple testing within each column. A, Correlations between changes ("deltas"). B, Correlations within cystectomy samples (post-treatment). C, Correlations within TUR-BT samples (pre-treatment). D, CD8⁺ T-cell percentage (mIF) fold change upon chemo-treatment between patient groups with the change in TNFα-via-NFκB gene signature score (RNA) below and higher than a median change. E, Fibroblast-derived TGF-β gene signature score (RNA) between groups of TUR-BT and cystectomy samples with the PD-L1 IC score lower and higher than the TUR-BT median and the cystectomy median correspondingly. F, Correlation between the fibroblast-derived TGF-β gene signature score (RNA) and CD8⁺-T-cell-to-cancer-cell 1-NN median distance (mIF) in cystectomy samples. G, CD8⁺-T-cell-to-cancer-cell 1-NN median

MVAC AND GEMCITABINE-CONTAINING PLATINUM-BASED REGIMENS WERE ASSOCIATED WITH DISTINCT CHANGES TO THE TIME

While all patients received platinum-based chemotherapy, the specific chemotherapeutic regimens varied (Fig. 1B). To assess the impact of these regimens on TIME changes, we explored differences between MVAC versus gemcitabine-containing platinum-based regimens. We used robust analogues of a mixed ANOVA with between-subject variable "chemo regimen" and within-subject variable "timepoint", i.e., TUR-BT (pre-treatment) or cystectomy (post-treatment; Methods, Statistical analysis). We performed this analysis with each of the target variables, which are the TIME characteristics changed upon chemotherapy ($CD8^+$ T-cell and macrophage cell percentages: Fig. 3A; PD-L1 IC, fibroblast TGF-β: Fig 2 D, G; $CD8^+$ T-cell-to-cancer median 1-NN distance, and macrophage-to-cancer median 1-NN distance: Fig. 3C). Besides significant coefficients for the timepoint term in all models (in line with the overall changes shown in Fig. 2 and 3), our analyses showed significant statistical interaction between the timepoint and chemo regimen variables in the models for the macrophage cell percentage and fibroblast TGF-β signaling (Fig. 5A). These results suggest that the change in macrophage cell percentage and fibroblast TGF-β signaling depended on the regimen, whereas the changes in $CD8^+$ T-cell density, PD-L1 IC, $CD8^+$ T-cell-to-cancer cell, and macrophage-to-cancer cell median 1-NN distances were the same for both regimens. The post-hoc analysis showed a more pronounced increase in the macrophage cell percentage upon MVAC than upon gemcitabine-containing chemotherapy (Fig. 5B). Conversely, fibroblast TGF-β signaling increased more upon the gemcitabine-containing platinum-based regimen (Fig. 5C). We did not find associations with the type of platinum agent (cisplatin versus carboplatin) for the six TIME characteristics analyzed before in the context of MVAC and gemcitabine-containing platinum-based regimens (Supplementary Fig. 8). However, the analysis for the platinum agent had less statistical power and a more unbalanced design due to the low number of carboplatin-treated patients (8 patients with paired mIF and 11 patients with paired RNA data) compared to the number of cisplatin-treated patients (68 patients with paired mIF and 57 patients with paired RNA data). pre- and post-treatment within groups of patients who received different chemotherapy regimens. The right panels show comparison between changes ("deltas") upon the distinct regimens.

In summary, our results show that platinum-based chemotherapy can induce changes that are potentially either pro-immunogenic (increased $CD8^+$ T-cell percentage, TNFα-via-NFκB signaling, IC PD-L1 score) or immune-inhibitory (larger distance of immune-to-cancer cells, stromal signatures).

A

Target variable	CD8⁺ T cell fraction (mIF)	Macrophage cell fraction (mIF)	PD-L1 IC	Fibroblast-derived TGFb signaling (ssGSEA score)	CD8⁺ T cell to cancer cell median 1-NN distance	Macrophage to cancer cell median 1-NN distance
Method	mixed ANOVA based on the trimmed means	F1-LD-F1 non-parametric model, ANOVA	F1-LD-F1 non-parametric model, ANOVA	mixed ANOVA based on the trimmed means	F1-LD-F1 non-parametric model, ANOVA	F1-LD-F1 non-parametric model, ANOVA
Chemo regimen, p-value	0.85	0.074	0.013	0.13	0.83	0.35
Time point, p-value	0.0056	0.00012	$1.0 * 10^{-5}$	$1.0 * 10^{-6}$	$3.2*10^{-7}$	$1.4*10^{-6}$
Chemo regimen: Time point, interaction p-value	0.66	**0.023**	0.13	**0.025**	0.84	0.66

B

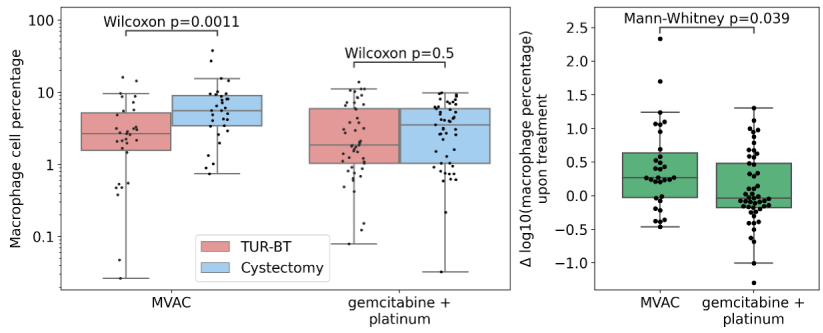

C

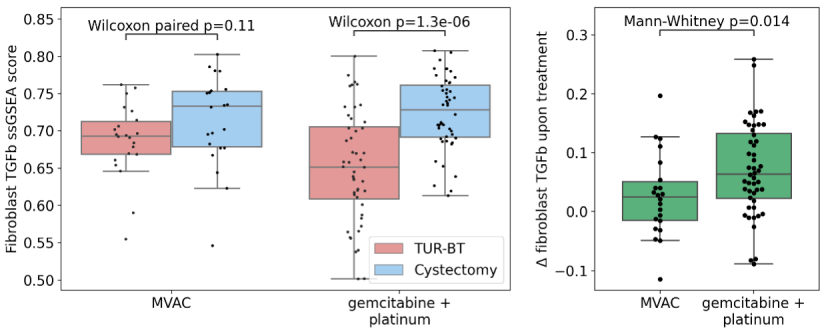

Figure 5 | Analysis of changes in the TIME characteristics upon MVAC and gemcitabine-containing platinum-based chemotherapy regimens. A, P-values of robust mixed ANOVA analogues are chosen depending on the data normality for each combination of the ANOVA design factors (Methods, Statistical analysis). Significant statistical interactions between the regimen and timepoint are highlighted as bold. **B,C**, Post-hoc analysis of changes in macrophage cell percentage (B) and fibroblast-derived TGF-β signaling (C). The left panels show comparison between pre- and post-treatment within groups of patients who received different chemotherapy regimens. The right panels show comparison between changes ("deltas") upon the distinct regimens.

DISCUSSION

The efficacy of concurrent chemotherapy and ICI has been established in lung, head-and-neck, triple-negative breast, gastric, and esophageal cancers[22]. In urothelial cancer, clinical trials yielded inconsistent results[6,7,8,11,12,23]. In this study, we comprehensively assessed the TIME in urothelial bladder cancer following platinum-based chemotherapy. To do so, we have collected and analyzed a large dataset of paired pre- and post-platinum-treatment bladder tumor samples analyzed with different experimental techniques.

In our cohort of MIBC patients treated with platinum-based chemotherapy, several parameters indicative of T-cell immunity increased. This included an increase in the $CD8^+$ T-cell percentage, as determined by mIF; the percentage of PD-$L1^+$ immune cells, determined by immunohistochemistry, and an upregulation of TNFα-via-NFκB, as shown in differential gene expression analysis. The macrophage ($CD68^+$) percentage increased as well, which appeared to be specifically associated with the MVAC treatment regimen.

Several preclinical studies suggested an association between cisplatin chemotherapy and increased $CD8^+$ T-cell infiltration or activation[24,25,26]. Single-cell RNA-seq analysis of peripheral blood immune cells of participants in the IMvigor130 trial at baseline and on chemotherapy demonstrated that cisplatin (and not carboplatin; both with gemcitabine) induced immune and inflammatory transcriptional programs in circulating monocytes including TNFα-via-NFκB and genes encoding proteins associated with antigen presentation and T-cell priming[10]. Seiler *et al*. found specific post-chemotherapy molecular subtypes in MIBC, some of which were characterized by higher immune signatures and $CD8^+$ T-cell immune infiltration[27]. In contrast, a recent study in human bladder cancer showed no association between neo-adjuvant platinum-based chemotherapy and $CD8^+$ T-cell infiltration assessed by mIF[28]. However, the sample size in the latter study (33 patients) was smaller than in our cohort and the comparison was made with raw cell densities (cells per mm^2) rather than percentages, potentially amplifying confounding signals from the different sample types (see Methods). Conversely, induction chemotherapy consisting of docetaxel, a platinum-containing agent and 5-fluorouracil induced PD-L1 expression and $CD8^+$ T-cell infiltration in patients with head and neck squamous cell carcinoma[29]. A similar effect was observed in connection to NAC with 5-fluorouracil and cisplatin in esophageal squamous cell carcinoma[30]. Further, in ovarian cancer, platinum- and taxane-based NAC regimens were associated with an increased T-cell infiltration and T-cell receptor (TCR) oligoclonal expansion both assessed via TCR-sequencing[31]. In triple-negative breast cancer, an induction therapy with doxorubicin was associated with an increase in inflammatory signatures, including TNFα-via-NFκB signaling[32].

In contrast to these alterations related to an enhanced immune presence in the tumor, potentially indicative of a favorable ICI response, several parameters previously connected to ICI resistance

increased upon chemotherapy. Expression of a fibroblast-derived TGF-β gene signature was enhanced after chemotherapy. Its upregulation was significantly higher in the tumors of patients treated with a gemcitabine-containing platinum-based regimen (in contrast to MVAC). In line with our results, a recent report suggests that platinum chemotherapy drug accumulation in cancer-associated fibroblasts intensified TGF-β activity and associated with increased cancer aggressiveness in colorectal cancer[33]. Additionally, median distances from $CD8^+$ T-cells and macrophages to their nearest neighboring cancer cell increased upon chemotherapy and were significantly correlated with the fibroblast-based TGF-β signaling in post-treatment samples. Interestingly, spatial analysis of triple-negative breast cancer in mice showed that quiescent cancer cells expressing chemotherapy resistance genes form niches which exclude immune infiltrates locally and contain immune-suppressive fibroblasts[34]. In our approach, local exclusion corresponds to the increase in 1-NN distances from immune cells to cancer cells.

Our findings may point to the importance of a balance between pro-immunogenic and anti-immunogenic aspects of the bladder cancer TIME, ultimately determining the response to ICI treatment. The importance of such opposing forces in the TIME was previously suggested by Wang *et al*.[19], showing that in patients with T-cell infiltrated tumors, higher EMT/stroma-related gene expression is associated with lower clinical benefit to nivolumab in advanced urothelial cancer. Similarly, Mariathasan *et al*[14] showed that a TGF-β in fibroblast-related signature was inversely associated with response to atezolizumab, specifically in immune-excluded tumors. Our findings suggest that platinum-based chemotherapy can modulate this balance, either in a positive or negative way.

The chemotherapy-associated TIME alterations discussed above suggest several potential avenues to improve benefit from chemotherapy and immunotherapy combinations. The addition of TGF-β inhibitors to ICI regimens after platinum-based NAC, especially in regimens containing gemcitabine, may potentially improve immunotherapeutic responses in MIBC. Combinations of ICI and TGF-β inhibitors have been tested in phase 1 and 2 clinical trials in various cancer types, including urothelial cancer[35]. However, while preclinical studies exploring the combination of TGF-β and PD-1/PD-L1 inhibition showed uniformly positive results, the addition of TGF-β inhibitors in clinical trials has often failed to show a meaningful benefit beyond the current generation of ICIs alone[35]. Administering agents promoting spatial rearrangement of immune cells to achieve closer proximity to cancer cells, e.g., bispecific antibodies, might be another treatment option specifically in the setting of ICI after platinum-based NAC. Several bispecific antibodies targeting cancer cells and T-cells have been tested in clinical urothelial cancer trials (e.g., Orlotamab (CD3×B7-H3)[36] and Catumaxomab (CD3 × EpCAM)[37]. Interestingly, therapeutic co-administration of TGF-β inhibitors and PD-L1 inhibitors in a mouse mammary carcinoma model recapitulating an immune-excluded phenotype was shown to facilitate T-cell penetration into the center of tumors and provoke tumor regression, while therapeutic blockade of PD-L1 or TGF-β alone had little or no effect[14].

This study has several limitations. First, we used different sample types for our analyses, which are transurethral resection (TUR-BT) samples as pre-chemotherapy tissue and radical cystectomy samples after chemotherapy. In our methods, we aimed to identify and mitigate possible biases in the mIF data analysis by comparing the total cell densities and the cell-type-agnostic 1-NN median distances between sample types and using cell percentages instead of raw densities. Another limitation is the heterogeneity in the chemotherapy regimens (Fig. 1B). Although the inclusion of different regimens could have allowed us to study divergent effects on the TIME by cisplatin vs. carboplatin, only 12% of patients were treated with carboplatin, while 78% received cisplatin. This complicated detecting TIME-related changes associated with the specific platinum agent, which are probable based on the recent findings from the translational analysis of the data from the IMvigor130 participants[10]. Further, although our ultimate interest was motivated by establishing potential synergy or antagonism between chemo- and immunotherapies, patients in our cohort did not receive immunotherapy peri-operatively. A dataset consisting of a pre- and post-NAC comprehensive TIME assessment and clinical data on additional peri-operative immunotherapy treatment does not exist currently. However, clinical studies randomizing between NAC with or without checkpoint inhibition are currently ongoing and tumor tissue collected in these trials may provide a source for further validation[38]. Finally, our study does not provide information whether the TIME modulation by chemotherapy is stable in time and affects the immune response to ICI at the time of its administration.

In conclusion, neo-adjuvant platinum-based chemotherapy for MIBC is associated with promoting TIME characteristics previously shown to relate to both ICI response ($CD8^+$ T-cell percentage, $PD\text{-}L1^+$ immune cell percentage) and ICI resistance (fibroblast-based TGF-β signaling, median distances from $CD8^+$ T-cells and macrophages to their nearest cancer cells). Additionally, our data suggests there may be biological differences between MVAC and gemcitabine-containing platinum-based chemo regimens in their effects on the bladder TIME. A better understanding of chemotherapy-induced changes in the bladder TIME and their implications for immunotherapy warrants further investigation. Future studies could test our hypotheses by analyzing data from patients randomized between NAC with and without concurrent ICI, with several ongoing phase 3 studies expected to provide relevant insights.

ACKNOWLEDGMENTS

We would like to thank all core facilities of the NKI for their help in this project and Charlotte Voskuilen and Elies Fransen van de Putte for their help in the collection of tumor samples. We would like to thank Auditi DebRoy from BMS for support in the project. The Research High Performance Computing (RHPC) facility is acknowledged for providing computational facilities to perform the analysis.

METHODS

PATIENT POPULATION

We retrospectively included patients that were treated with neoadjuvant chemotherapy followed by radical cystectomy for MIBC (cT2-4N0-3). Only patients with remaining viable tumor tissue after cystectomy were included (≥ypT1), regardless of nodal status. Exclusion criteria were prior pelvic radiotherapy and non-urothelial primary histology. Urothelial carcinoma with squamous and/or glandular differentiation was allowed. Patients underwent radical cystectomy between 1995 and 2021. Follow-up was performed according to local guidelines. Data were collected in accordance with institutional and national ethical guidelines; the project was approved by the NKI institutional review board (IRBm20-296).

TISSUE COLLECTION AND RNA ISOLATION

Pre-treatment TUR-BT and post-treatment cystectomy material was stored as formalin-fixed paraffin embedded (FFPE) tissue blocks in The Netherlands Cancer Institute. Tumor material from patients that had their TUR-BT or cystectomy in a different hospital was requested as tissue blocks and subsequently stored at The Netherlands Cancer Institute. An experienced uro-pathologist assessed all available tissue blocks and the most representative tissue block was selected. Tumor area and tumor cell percentage was determined by an experienced uro-pathologist. RNA was isolated from baseline tumor material (5-10x 10 µm slides) using the using the Qiagen AllPrep FFPE DNA/RNA Kit.

RNA SEQUENCING

Quality and quantity of the total RNA were assessed using the 2100 Bioanalyzer and a Nano chip (Agilent). The percentage of RNA fragments with > 200-nucleotide fragment distribution values (DV200) were determined using the region analysis method according to the manufacturer's instructions manual (Illumina, technical-note-470-2014-001). Strand-specific libraries were generated using the TruSeq RNA exome library prep kit (Illumina) according to the manufacturer's instructions (Illumina, 1000000039582v01). Briefly, total RNA was random primed and reverse transcribed using SuperScript II reverse transcriptase (Invitrogen, 18064-014) with the addition of actinomycin D. Second strand synthesis was performed using polymerase I and RNaseH with the replacement of dTTP for dUTP. The generated cDNA fragments were 3'-end adenylated and ligated to Illumina (batch 1, 140 samples) or Integrated DNA Technologies xGen UDI(10bp)-UMI(9bp; batch 2, 35 samples) paired-end sequencing adapters and subsequently amplified by 15 cycles of PCR. The libraries were validated on a 2100 Bioanalyzer using a 7500 chip (Agilent) followed by a 1-4 plex library pooling containing up to 200 ng of each sample. The pooled libraries were enriched for target regions using the probe Coding Exome Oligos set (CEX, 45MB) according to the manufactures instruction (Illumina, 1000000039582v01). Briefly, cDNA libraries and biotin- labeled capture probes were combined and hybridized using a denaturation step of 95°C for 10 minutes and an incubation step from 94 °C to 58 °C with a ramp of 18 cycles, a 1-minute incubation and 2

°C per cycle. The hybridized target regions were captured using streptavidin magnetic beads and subjected to two stringency washes, an elution step and a second round of enrichment followed by a cleanup using AMPure XP beads (Beckman, A63881) and PCR amplification of 10 cycles. The target enriched pools were analyzed on a 2100 Bioanalyzer using a 7500 chip (Agilent), diluted and subsequently pooled equimolar into a multiplex sequencing pool. The libraries from 140 samples originated from 74 patients (batch 1) were sequenced with 65-bp single-end reads on a HiSeq 2500 using V4 chemistry (Illumina). The libraries from additional 35 samples (from the other 25 patients, batch 2) were sequenced with 54-bp paired-end reads on a NovaSeq 6000 using an SP Reagent Kit v1.5 (100cycles; Illumina).

IMMUNOHISTOCHEMISTRY AND MULTIPLEX IMMUNOFLUORESCENCE

Immunohistochemistry of the FFPE tumor samples was performed on a BenchMark Ultra autostainer (Ventana Medical Systems). Briefly, paraffin sections were cut at 3 um, heated at 75°C for 28 minutes and deparaffinized in the instrument with EZ prep solution (Ventana Medical Systems). Heat-induced antigen retrieval was carried out using Cell Conditioning 1 (CC1, Ventana Medical Systems) for 48 minutes at 95°C. PD-L1 was detected using clone 22C3 (1/40 dilution, 1 hour at RT, Agilent/DAKO). Bound antibody was detected using the OptiView DAB Detection Kit (Ventana Medical Systems). Slides were counterstained with Hematoxylin and Bluing Reagent (Ventana Medical Systems). A PANNORAMIC® 1000 scanner from 3DHISTECH was used to scan the slides at a 40x magnification. After scanning, PD-L1 and hematoxylin and eosin slides were uploaded to Slide Score (www.slidescore.com) for manual scoring. An experienced uro-pathologist determined the percentage of PD-L1 positive tumor cells (TC), the percentage of PD-L1 positive immune cells (IC) and the combined positivity score (CPS). Analysis of tumor immune cell infiltrates (anti-CD3 (1:400 dilution Clone P7, Thermo Fisher Scientific), anti-CD8 (1:100 dilution Clone C8/144B, Dako), anti-CD68 (1:500 dilution Clone KP1, Dako), anti-FoxP3 (1:50 dilution Clone 236A/47, Abcam), anti-CD20 (1:500 dilution Clone L26, Dako) and anti-PanCK (1:100 dilution Clone AE1AE3, Thermo Fisher Scientific) was performed by multiplex immunofluorescence technology on a Ventana Discovery Ultra automated stainer using PerkinElmer opal seven-color dyes. In short, 3 µm FFPE sections were cut and heated at 75 °C for 28 minutes and subsequently deparaffinized in EZ Prep solution (Ventana Medical Systems). Using Cell Conditioning 1 (CC1, Ventana Medical Systems), heat-induced antigen retrieval was conducted at 95 °C for 32 minutes. Further analysis was done by VECTRA image acquisition (Akoya Biosciences, v3.0) and HALO (Indica Labs, v2.3) image analysis. Tumor and stroma regions were classified by HALO automated tissue segmentation primarily based on PanCK expression. Adjacent stroma was defined as all tissue surrounding the tumor area within 150 µm. Cell segmentation was performed using a pre-trained nuclear segmentation AI module in HALO. Marker thresholds were set manually for each sample. Data was analyzed separately for tumor and stroma regions and subsequently exported. Immune cell classification was based on marker expression, as shown in the table below. When a cell was positive for two or more mutually exclusive markers, the cell was classified according to the highest relative intensity of the respective markers.

Marker positivity[a]	Cell type
PanCK$^+$	Cancer cell
CD8$^+$ FoxP3$^-$	CD8$^+$ T-cell
CD8$^-$ FoxP3$^+$	Treg
CD3$^+$CD8$^-$FoxP3$^-$	T-helper
CD68$^+$	Macrophage
CD20$^+$	B-cell

[a] all cells are DAPI positive

COMPUTATIONAL ANALYSIS OF MULTIPLEX IMMUNOFLUORESCENCE DATA

Final classification of cells into tumor and stromal regions and quantification of these regions' areas was performed by the method we previously published[21] with the modification to take into account immune cells in addition to the negative cells while computing stroma-related kernel density estimation (KDE). Initially, cell densities were obtained from the output of this step by dividing cell counts over the corresponding area. The density of the total cells (regardless of their label) was significantly higher in TUR-BT samples than in cystectomy (Supplementary Fig. 2A). To minimize the possible bias related to the sample type, we switched to cell percentages by dividing each cell density over the total cell density. We quantified spatial relationships by using the first-nearest neighbor statistics. After quantifying distances between the first nearest neighboring cells of differenT-cell types in the full analyzed area (tumor plus adjacent stroma), we fitted the Weibull distribution to these data using the generalized linear mixed effect models for each of 49 cell phenotype combination in our mIF data following[21]. The scale and shape parameters were used to calculate medians of the Weibull distribution. Before analyzing the medians, we performed the same analysis with the cell labels removed and compared the medians between the two sample types to control for a possible bias. These overall medians were the same between the sample types (Supplementary Fig. 2B).

RNA-SEQ COMPUTATIONAL ANALYSIS

Gene expressions were quantified with Kallisto (v0.46.1) with the Gencode reference transcriptome v40 (basic annotation). Gene TPM values were filtered according to the gene biotype from the GTF (General Transfer Format) transcriptome annotation file, renormalized to 1 million in total, and used for ssGSEA (Gseapy v0.10.7). The following types of genes (according to the Gencode GTF basic annotation, v40) were retained in the expression files: 'protein_coding', 'processed_pseudogene', 'transcribed_processed_pseudogene','TEC', 'polymorphic_pseudogene', 'pseudogene', 'IG_C_gene','TR_C_gene','translated_processed_pseudogene', 'IG_C_pseudogene'. Transcript counts were summarized to the gene level and used for differential expression with DESeq2 (v1.36.0) and GSEA with Fgsea (v1.22.0) and Msigdbr (v7.5.1). The dataset included two batches with differences in the library preparation protocol and sequencing. The batch correction procedure was performed with the Limma R package (v3.52.4, function removeBatchEffect) on logarithmed gene TPM expressions.

STATISTICAL ANALYSIS

Pandas v1.3.3 and NumPy v1.20.0 were used for data handling. Seaborn v0.12.2, Matplotlib v3.7.3, statannotations 0.4.2, and EnhancedVolcano v1.14.0 were used for plotting. Basic statistical tests were implemented from Scipy v1.8.1 and Statsmodels v0.13.1. Before comparison, Kendall τ-*b* correlation coefficients were transformed to the equivalent Pearson R using Kendall's formula[39]. Function r.test from R package Psych (v2.3.9) was used to perform z-test of the difference of the Fisher's z-transformed correlations divided by the standard error of the difference. For the analysis of association between different chemotherapy regimens and changes in the TIME, we used robust analogues of a mixed ANOVA: a rank-based nonparametric method for longitudinal data in factorial experiments (F1-LD-F1 design[40], R package nparLD, v2.2) and the robust mixed ANOVA based on the trimmed means[41] (R package WRS2, v1.1.5). For the variables violating the assumption of normality within each combination of the ANOVA model factors (macrophage cell percentage, CD8+ T-cell/macrophage to cancer cell median 1-NN distances, and PD-L1 IC), we applied the non-parametric method. The normality was tested with Shapiro-Wilk test implemented in R package Rstatix (v0.7.2).

DATA AVAILABILITY

RNA sequencing data have been deposited in the European Genome-phenome Archive under the accession code EGASXXX and will be made available upon reasonable request for academic use and within the limitations of the provided informed consent by the corresponding author upon acceptance. Every request will be reviewed by the institutional review board of the Netherlands Cancer Institute; the researcher will need to sign a data access agreement with the Netherlands Cancer Institute after approval. Multiplex immunofluorescence primary data used for this study will be made available upon reasonable academic request within the limitations of informed consent by the corresponding author upon acceptance.

REFERENCES

1. Witjes JA, Bruins HM, Cathomas R, Compérat EM, Cowan NC, Gakis G, et al. European Association of Urology Guidelines on Muscle-invasive and Metastatic Bladder Cancer: Summary of the 2020 Guidelines. Eur Urol. 2021 Jan;79(1):82-104.
2. Powles T, Bellmunt J, Comperat E, De Santis M, Huddart R, Loriot Y, et al.; ESMO Guidelines Committee. Bladder cancer: ESMO Clinical Practice Guideline for diagnosis, treatment and follow-up. Ann Oncol. 2022 Mar;33(3):244-258.
3. Yin M, Joshi M, Meijer RP, Glantz M, Holder S, Harvey HA, et al. Neoadjuvant Chemotherapy for Muscle-Invasive Bladder Cancer: A Systematic Review and Two-Step Meta-Analysis. *Oncologist* 2016;21: 708-15.
4. Pfister C, Gravis G, Fléchon A, Soulié M, Guy L, Laguerre B, et al.; VESPER Trial Investigators. Randomized Phase III Trial of Dose-dense Methotrexate, Vinblastine, Doxorubicin, and Cisplatin, or Gemcitabine and Cisplatin as Perioperative Chemotherapy for Patients with Muscle-invasive Bladder Cancer. Analysis of the GETUG/AFU V05 VESPER Trial Secondary Endpoints: Chemotherapy Toxicity and Pathological Responses. Eur Urol. 2021 Feb;79(2):214-221.
5. Advanced Bladder Cancer (ABC) Meta-analysis Collaboration. Neoadjuvant chemotherapy in invasive bladder cancer: update of a systematic review and meta-analysis of individual patient data advanced bladder cancer (ABC) meta-analysis collaboration. Eur Urol. 2005 Aug;48(2):202-5; discussion 205-6.
6. Bajorin DF, Witjes JA, Gschwend JE, Schenker M, Valderrama BP, Tomita Y, et al. Adjuvant Nivolumab versus Placebo in Muscle-Invasive Urothelial Carcinoma. N Engl J Med. 2021 Jun 3;384(22):2102-2114. Erratum in: N Engl J Med. 2021 Aug 26;385(9):864.
7. Powles T, Park SH, Voog E, Caserta C, Valderrama BP, Gurney H, et al. Avelumab Maintenance Therapy for Advanced or Metastatic Urothelial Carcinoma. N Engl J Med. 2020 Sep 24;383(13):1218-1230.
8. Galsky MD, Arija JÁA, Bamias A, Davis ID, De Santis M, Kikuchi E, et al.; IMvigor130 Study Group. Atezolizumab with or without chemotherapy in metastatic urothelial cancer (IMvigor130): a multicentre, randomised, placebo-controlled phase 3 trial. Lancet. 2020 May 16;395(10236):1547-1557.
9. Galsky M, Arija J, De Santis M, Davis I, Bamias A, Kikuchi E, et al. Atezolizumab (atezo) + platinum/gemcitabine (plt/gem) vs placebo + plt/gem for first-line (1L) treatment (tx) of locally advanced or metastatic urothelial carcinoma (mUC): Final OS from the randomized Phase 3 IMvigor130 study. Journal of Clinical Oncology 2023 41:6_suppl, LBA440.
10. Galsky MD, Guan X, Rishipathak D, Rapaport AS, Shehata HM, Banchereau R, et al. Immunomodulatory effects and improved outcomes with cisplatin- versus carboplatin-based chemotherapy plus atezolizumab in urothelial cancer. Cell Rep Med. 2024 Feb 20;5(2):101393.
11. van der Heijden MS, Sonpavde G, Powles T, Necchi A, Burotto M, Schenker M, et al.; CheckMate 901 Trial Investigators. Nivolumab plus Gemcitabine-Cisplatin in Advanced Urothelial Carcinoma. N Engl J Med. 2023 Nov 9;389(19):1778-1789.
12. Powles T, Csőszi T, Özgüroğlu M, Matsubara N, Géczi L, Cheng SY, et al.; KEYNOTE-361 Investigators. Pembrolizumab alone or combined with chemotherapy versus chemotherapy as first-line therapy for advanced urothelial carcinoma (KEYNOTE-361): a randomised, open-label, phase 3 trial. Lancet Oncol. 2021 Jul;22(7):931-945.
13. Go, Ronald S., and Alex A. Adjei. "Review of the comparative pharmacology and clinical activity of cisplatin and carboplatin." *Journal of Clinical Oncology* 17.1 (1999): 409-409.
14. Mariathasan S, Turley SJ, Nickles D, Castiglioni A, Yuen K, Wang Y, et al. TGFβ attenuates tumour response to PD-L1 blockade by contributing to exclusion of T cells. Nature. 2018 Feb 22;554(7693):544-548.
15. Powles T, Kockx M, Rodriguez-Vida A, Duran I, Crabb SJ, Van Der Heijden MS, et al. Clinical efficacy and biomarker analysis of neoadjuvant atezolizumab in operable urothelial carcinoma in the ABACUS trial. Nat Med. 2019 Nov;25(11):1706-

1714. Erratum in: Nat Med. 2020 Jun;26(6):983. Erratum in: Nat Med. 2023 Dec;29(12):3271.

16. Ayers M, Lunceford J, Nebozhyn M, Murphy E, Loboda A, Kaufman DR, et al. IFN-γ-related mRNA profile predicts clinical response to PD-1 blockade. J Clin Invest. 2017 Aug 1;127(8):2930-2940.
17. van Dijk N, Gil-Jimenez A, Silina K, Hendricksen K, Smit LA, de Feijter JM, et al. Preoperative ipilimumab plus nivolumab in locoregionally advanced urothelial cancer: the NABUCCO trial. Nat Med. 2020 Dec;26(12):1839-1844.
18. Liberzon A, Birger C, Thorvaldsdóttir H, Ghandi M, Mesirov JP, Tamayo P. The Molecular Signatures Database (MSigDB) hallmark gene set collection. Cell Syst. 2015 Dec 23;1(6):417-425.
19. Wang L, Saci A, Szabo PM, Chasalow SD, Castillo-Martin M, Domingo-Domenech J, et al. EMT- and stroma-related gene expression and resistance to PD-1 blockade in urothelial cancer. Nat Commun. 2018 Aug 29;9(1):3503.
20. Vos JL, Elbers JBW, Krijgsman O, Traets JJH, Qiao X, van der Leun AM, et al. Neoadjuvant immunotherapy with nivolumab and ipilimumab induces major pathological responses in patients with head and neck squamous cell carcinoma. Nat Commun. 2021 Dec 22;12(1):7348.
21. Gil-Jimenez A, van Dijk N, Vos JL, Lubeck Y, van Montfoort ML, Peters D, et al. Spatial relationships in the urothelial and head and neck tumor microenvironment predict response to combination immune checkpoint inhibitors. bioRxiv 2023.05.25.542236.
22. Larroquette M, Domblides C, Lefort F, Lasserre M, Quivy A, Sionneau B, et al. Combining immune checkpoint inhibitors with chemotherapy in advanced solid tumours: A review. Eur J Cancer. 2021 Oct 13;158:47-62.
23. Bellmunt J, Hussain M, Gschwend JE, Albers P, Oudard S, Castellano D, et al.; IMvigor010 Study Group. Adjuvant atezolizumab versus observation in muscle-invasive urothelial carcinoma (IMvigor010): a multicentre, open-label, randomised, phase 3 trial. Lancet Oncol. 2021 Apr; 22(4):525-537.
24. Wakita D, Iwai T, Harada S, Suzuki M, Yamamoto K, Sugimoto M. Cisplatin Augments Antitumor T-Cell Responses Leading to a Potent Therapeutic Effect in Combination With PD-L1 Blockade. Anticancer Res (2019) 39:1749–60.
25. Markasz L, Skribek H, Uhlin M, Otvos R, Flaberg E, Eksborg S, et al. Effect of frequently used chemotherapeutic drugs on cytotoxic activity of human cytotoxic T-lymphocytes. J Immunother. 2008 Apr;31(3):283-93.
26. Beyranvand Nejad E, van der Sluis TC, van Duikeren S, Yagita H, Janssen GM, van Veelen PA, et al. Tumor Eradication by Cisplatin Is Sustained by CD80/86-Mediated Costimulation of CD8+ T Cells. Cancer Res. 2016 Oct 15;76(20):6017-6029.
27. Seiler R, Gibb EA, Wang NQ, Oo HZ, Lam HM, van Kessel KE, et al. Divergent Biological Response to Neoadjuvant Chemotherapy in Muscle-invasive Bladder Cancer. Clin Cancer Res. 2019 Aug 15;25(16):5082-5093.
28. van Wilpe S, Sultan S, Gorris MAJ, Somford DM, Kusters-Vandevelde HVN, Koornstra RHT, et al. Intratumoral T cell depletion following neoadjuvant chemotherapy in patients with muscle-invasive bladder cancer is associated with poor clinical outcome. Cancer Immunol Immunother. 2023 Jan;72(1):137-149.
29. Leduc C, Adam J, Louvet E, Sourisseau T, Dorvault N, Bernard M, et al. TPF induction chemotherapy increases PD-L1 expression in tumour cells and immune cells in head and neck squamous cell carcinoma. ESMO Open. 2018 Jan 9;3(1):e000257.
30. Fukuoka E, Yamashita K, Tanaka T, Sawada R, Sugita Y, Arimoto A, et al. Neoadjuvant Chemotherapy Increases PD-L1 Expression and CD8+ Tumor-infiltrating Lymphocytes in Esophageal Squamous Cell Carcinoma. Anticancer Res. 2019 Aug;39(8):4539-4548.
31. Jiménez-Sánchez A, Cybulska P, Mager KL, Koplev S, Cast O, Couturier DL, et al. Unraveling tumor-immune heterogeneity in advanced ovarian cancer uncovers immunogenic effect of chemotherapy. Nat Genet. 2020 Jun;52(6):582-593.
32. Voorwerk L, Slagter M, Horlings HM, Sikorska K, van de Vijver KK, de Maaker M, et al. Immune induction strategies in

metastatic triple-negative breast cancer to enhance the sensitivity to PD-1 blockade: the TONIC trial. Nat Med. 2019 Jun;25(6):920-928.

33. Linares J, Sallent-Aragay A, Badia-Ramentol J, Recort-Bascuas A, Méndez A, Manero-Rupérez N, et al. Long-term platinum-based drug accumulation in cancer-associated fibroblasts promotes colorectal cancer progression and resistance to therapy. Nat Commun. 2023 Feb 10;14(1):746.
34. Baldominos P, Barbera-Mourelle A, Barreiro O, Huang Y, Wight A, Cho JW, et al. Quiescent cancer cells resist T cell attack by forming an immunosuppressive niche. Cell. 2022 May 12;185(10):1694-1708.e19.
35. Metropulos AE, Munshi HG, Principe DR. The difficulty in translating the preclinical success of combined TGFβ and immune checkpoint inhibition to clinical trial. EBioMedicine. 2022 Dec;86:104380.
36. Blanco B, Domínguez-Alonso C, Alvarez-Vallina L. Bispecific Immunomodulatory Antibodies for Cancer Immunotherapy. *Clin Cancer Res*. 2021; 27(20): 5457–5464.
37. Ruf P, Bauer HW, Schoberth A, Kellermann C, Lindhofer H. First time intravesically administered trifunctional antibody catumaxomab in patients with recurrent non-muscle invasive bladder cancer indicates high tolerability and local immunological activity. *Cancer Immunol Immunother*. 2021; 70(9): 2727–2735.
38. Sonpavde G, Necchi A, Gupta S, Steinberg GD, Gschwend JE, Van Der Heijden MS, et al. ENERGIZE: a Phase III study of neoadjuvant chemotherapy alone or with nivolumab with/without linrodostat mesylate for muscle-invasive bladder cancer. Future Oncol. 2020 Jan;16(2):4359-4368.
39. Kendall, M. G. (1970). Rank correlation methods (4th ed.). London: Charles Griffin & Co. Page 126.
40. Noguchi, K., Gel, Y. R., Brunner, E., & Konietschke, F. (2012). nparLD: An R Software Package for the Nonparametric Analysis of Longitudinal Data in Factorial Experiments. Journal of Statistical Software, 50(12), 1–23.
41. Mair P, Wilcox RR (2020). "Robust Statistical Methods in R Using the WRS2 Package." *Behavior Research Methods*, 52, 464–488.

SUPPLEMENTARY DATA

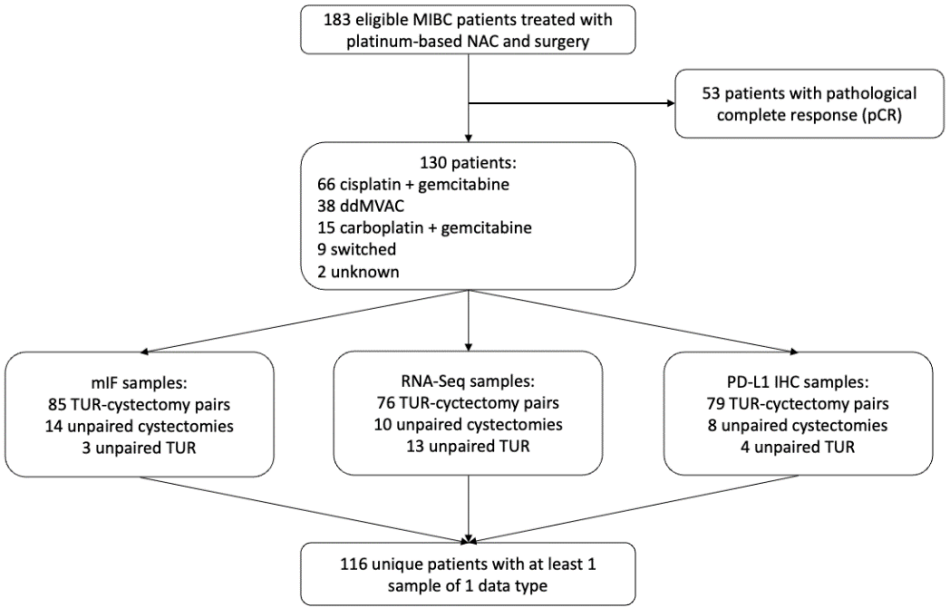

Supplementary Figure 1 | Consort diagram.

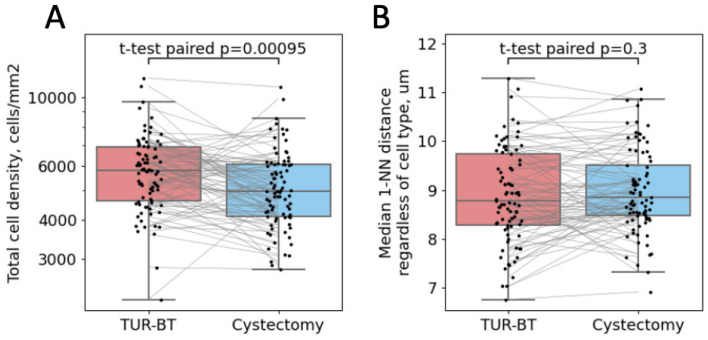

Supplementary Figure 2 | Evaluating the sample-type-related bias in the mIF data. A, Comparison of the total cell density between the sample types. **B**, Comparison of the median 1-NN distances between cells regardless of their type.

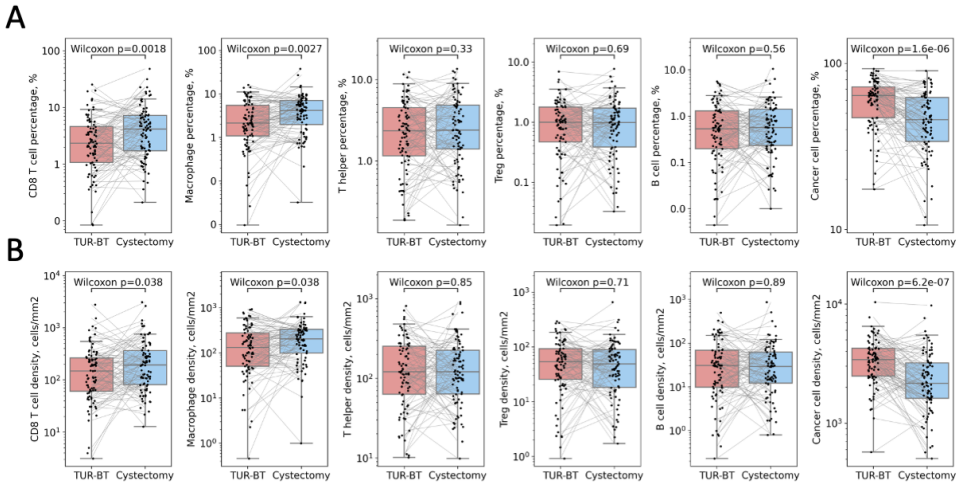

Supplementary Figure 3 | Changes in cell percentages. **A**, and cell densities **B**, associated with platinum-based chemotherapy for all cell types identified by our mIF panel (Methods).

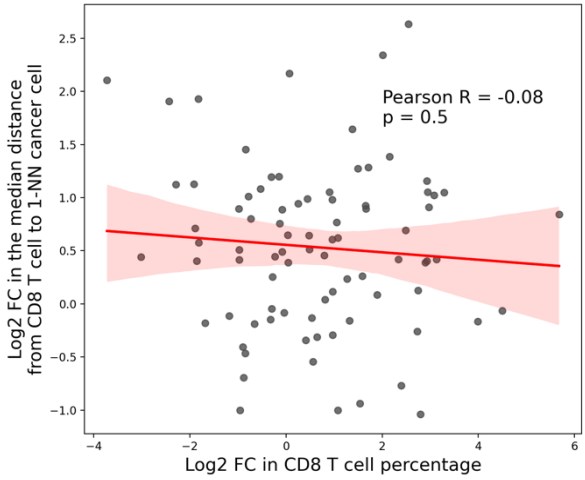

Supplementary Figure 4 | Correlation between Log2 fold changes in CD8⁺ T cell percentage and in the median distance from CD8⁺ T cells to their 1-NN cancer cells upon chemotherapy. One extreme distance outlier (higher than Q3 + 3IQR, where Q3 is the third quartile and IQR is the interquartile range) was excluded due to containing only two CD8⁺ T cells.

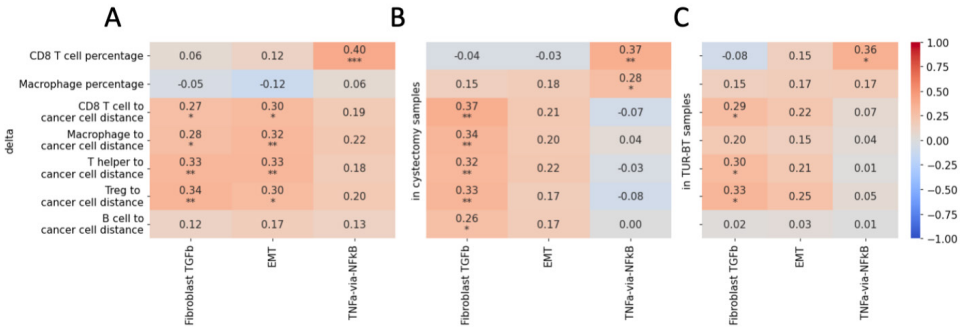

Supplementary Figure 5 | Correlation analysis of parameters altered by the chemo-treatment between different data modalities. RNA-Seq is shown on x-axis; mIF and IHC are shown on y-axis. Pearson correlation coefficients are shown. Stars denote p-values for the correlation coefficients to be non-zero assessed by the distribution of (two-sided test): $P<0.05$ (*); $P<0.01$ (**); $P<0.001$ (***). P-values are FDR-adjusted for multiple testing within each column. **A**, Correlations between changes ("deltas"). **B**, Correlations within cystectomy samples (post-treatment). **C**, Correlations within TUR-BT samples (pre-treatment).

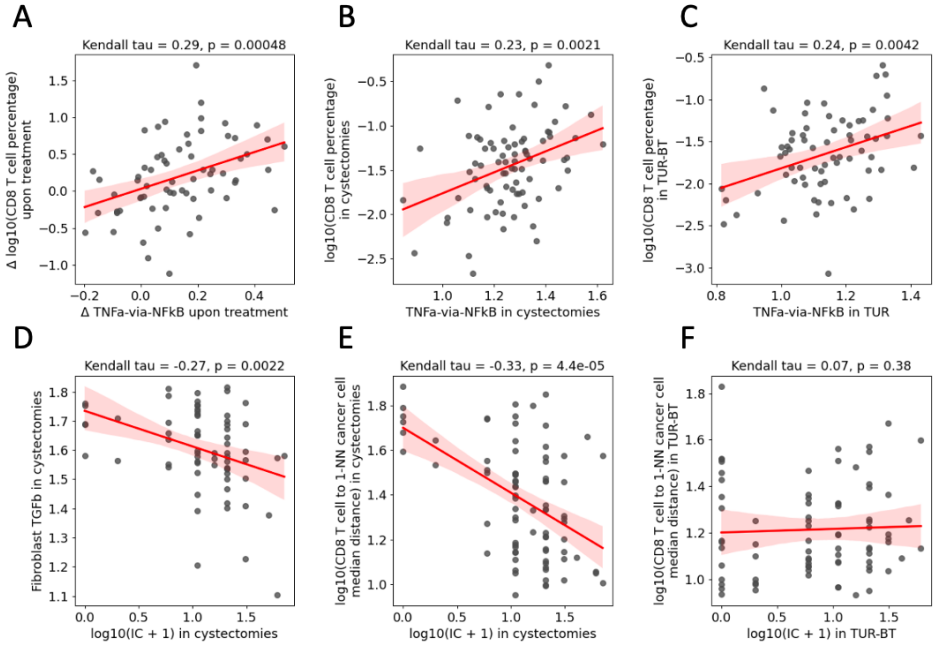

Supplementary Figure 6 | Correlations of the selected TME characteristics altered by chemo-treatment. **A-C**, Correlations between CD8 T-cell percentage (mIF) and TNFα-via-NFκB gene signature score (RNA) for changes, cystectomy samples, and TUR-BT samples. **D**, Correlation between PD-L1^{+} immune cell percentage and fibroblast-derived TGF-β signaling in cystectomy samples. **E,F**, Correlations between CD8^{+} T-cell-to-cancer-cell 1-NN median distance and PD-L1^{+} immune cell percentage for cystectomy and TUR-BT samples.

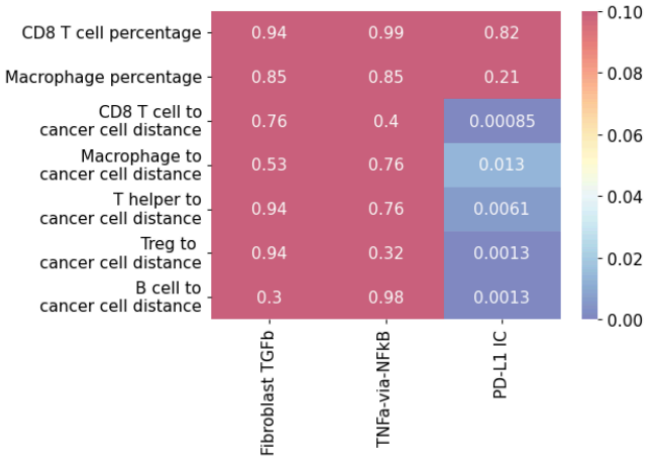

Supplementary Figure 7 | FDR-corrected p-values for comparison of Kendall □ correlation coefficients (Methods, Statistical analysis) between cystectomy and TUR-BT sample sets.

Target variable	$CD8^+$ T cell fraction (mIF)	Macrophage cell fraction (mIF)	PD-L1 IC	Fibroblast-derived TGFb signaling (ssGSEA score)	$CD8^+$ T cell to cancer cell median 1-NN distance	Macrophage to cancer cell median 1-NN distance
Method	mixed ANOVA based on the trimmed means	F1-LD-F1 non-parametric model, ANOVA	F1-LD-F1 non-parametric model, ANOVA	F1-LD-F1 non-parametric model, ANOVA	F1-LD-F1 non-parametric model, ANOVA	F1-LD-F1 non-parametric model, ANOVA
Platinum agent, p-value	0.09	0.0019	0.80	0.68	0.84	0.78
Time point, p-value	0.009	0.0069	$2.3 * 10^{-6}$	$1.6 * 10^{-9}$	$2.0*10^{-6}$	$2.6*10^{-9}$
Platinum agent: Time point, interaction p-value	0.12	0.61	0.39	0.15	0.50	0.11

Supplementary Figure 8 | Analysis of changes in the TME characteristics upon chemotherapy with cisplatin and carboplatin. P-values of mixed ANOVA or its robust analogues (depending on the violation of the default mixed ANOVA assumptions of normality, homoscedasticity, and homogeneity of covariances).